Supporting information for: Mode-Specificity of Vibrationally Coherent Internal Conversion in Rhodopsin during the Primary Visual Event

Christoph Schnedermann, Matz Liebel, and Philipp Kukura*

Physical and Theoretical Chemistry Laboratory, Oxford University, South Parks Road, Oxford OX1 3QZ, U.K.

E-mail: philipp.kukura@chem.ox.ac.uk

Data Processing

All traces were corrected for white light chirp by fitting the coherent artifact of pure water to a third order polynomial.[S1] For the resonant experiment, this was followed by a global subtraction algorithm of the electronic background to obtain pure coherence maps. The traces were subsequently truncated at a time delay of +80 fs to avoid contamination by the coherent artifact.[S2] Prior Fourier transformation, we applied a Kaiser window to reduce peak ringing. The application of a Kaiser window significantly improved the spectral appearance and resolution together with zero-padding, but also suppressed any signatures of time-dependent frequency changes on the product surface as reported previously.[S3] To enable a meaningful comparison with resonance Raman (RR) data, the resulting coherence maps

*To whom correspondence should be addressed

were multiplied by a wavelength-dependent time resolution curve which takes into account the temporal walk-off between the pump and the probe pulse in the flowcell.

Effective Time Resolution

A chirped WL probe pulse with a transform limit of ∼4 fs was used in combination with an 8 fs on-resonant and a 9 fs off-resonant pump pulse. The temporal profiles retrieved by SHG-FROG are shown in Figure S1.

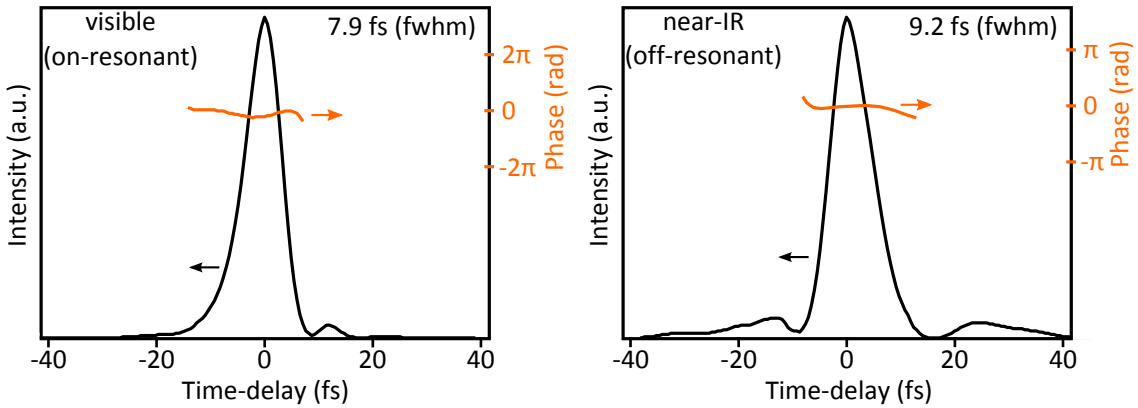

Figure S1: Temporal profiles of on-resonant (left) and off-resonant (right) pump pulses retrieved with SHG-FROG.

With these pulses we are able to resolve vibrational modes up to 3000 cm^{-1} for rhodopsin as shown in Figure S2 providing an effective time resolution as low as 11 fs.[S1,S4] The observed high-frequency bands >2000 cm^{-1} are likely combination bands suggesting, that the retrieved Fourier spectra originate from hot rhodopsin/bathorhodopsin.

Time-Resolution Scaling

The vibrational coherences recorded in transient absorption spectroscopy are necessarily convolved with the instrument response function (IRF), representative of the time resolution of the experiment at a given wavelength. This results in an underestimation of the coherent activity in the high-frequency window of a Fourier transform (FFT) spectrum.[S1,S5] Therefore,

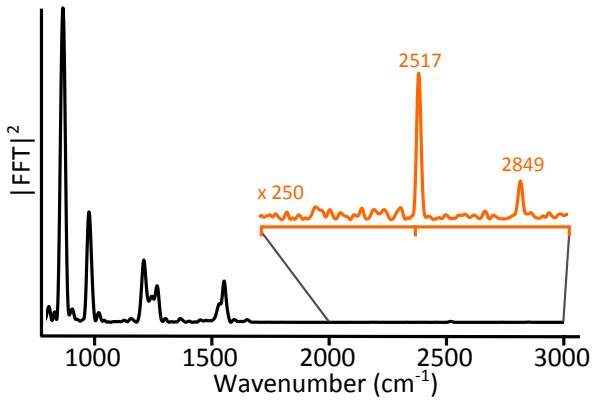

Figure S2: Fourier power spectrum averaged from 580 - 640 nm obtained after resonant excitation by an 8 fs pulse. Raman modes up to 3000 cm^{-1} are visible suggesting an effective time resolution of 11 fs.

we approximated the IRF as a Gaussian function with a full-width-half-maximum (fwhm) corresponding to the time resolution obtained from the temporal walk-off of pump and probe pulse in the sample cell. We subsequently calculated a frequency-dependent scaling factor translating the FFT-amplitude of a convolved oscillation of given frequency into an unconvolved FFT-signal, thus allowing for a more reliable intensity comparison with RR. This approach is validated by the comparison of the off-resonant experiment with the RR spectrum of rhodopsin as shown in the main text (Figure 3).

To obtain the wavelength-dependent time resolution (Figure S3a) we calculated the effective pulse broadening of the pump pulse in the sample cell using the normalized pump spectrum and the wavelength-dependent refractive index of the solvent. Accounting for the absorption of the pump as a function of path length we obtain a mean pump pulse duration for the experiment. The probe pulse is an uncompressed WL continuum of 300 fs duration but as a consequence of dispersed detection the relevant probe duration equals its transform limit of 4 fs.[S1,S6] Convolving two Gaussian envelopes with mean pump and probe durations leads to the initial time resolution of the experiment at the center frequency of the pump pulse. We further factored in the wavelength dependence of the refractive index of the sample, i.e. the group-velocity-mismatch between pump and probe, ignoring the negligible spatial walk-off arising from a non-zero crossing angle. Additionally including pump

depletion in the sample cell due to absorption yields the effective wavelength-dependent time resolution used for the final scaling of the obtained Fourier amplitudes (Figure S3b).

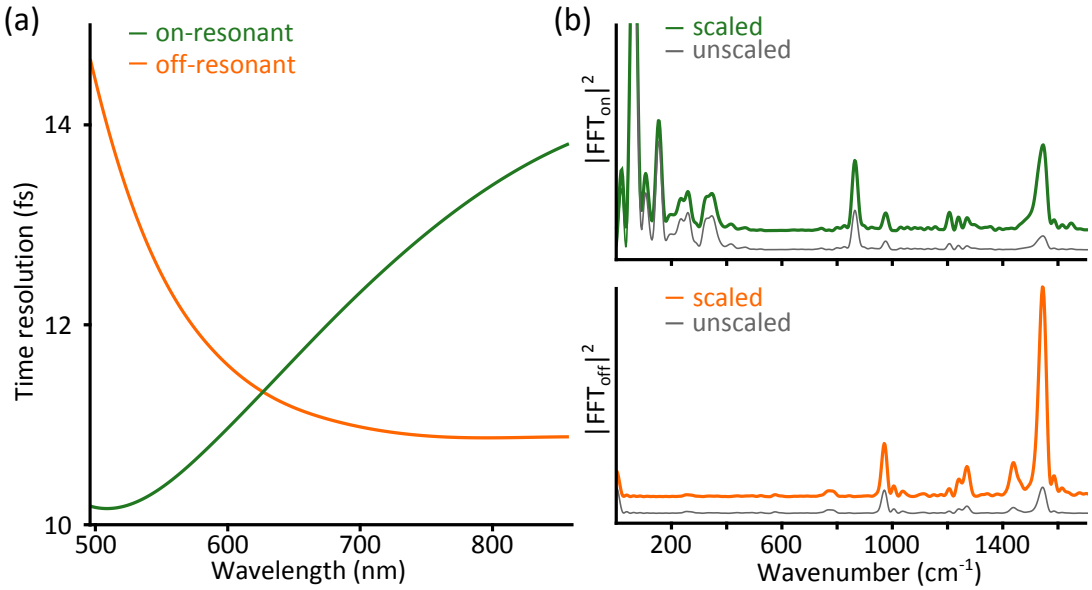

Figure S3: Overview over time-resolution scaling. (a) Wavelength-dependent time resolution for on-resonant and off-resonant excitation. (b) Comparison of averaged spectra with and without time-resolution scaling, offset for clarity. Top: on-resonant, bottom: off-resonant.

Wavelength Dependence of Resonance Raman Spectra

The comparison of resonance Raman spectra (488 nm[S7] and 805 nm[S3]) to time-domain Raman spectra (averaged around 600 nm) carried out in the main text (Figure 3) requires, that the Raman spectra of rhodopsin and bathorhodopsin do not change significantly as the resonance Raman excitation wavelength is changed. Comparison of available literature spectra (Figure S4) and the spectra presented in Figure 3 shows that the Raman spectra of rhodopsin and bathorhodopsin indeed remain nearly unaltered as the probe wavelength is altered. We note in particular that all bands remain visible as a function of excitation wavelength. This is a strong indication, that observed differences between our time-domain Raman spectra and the resonance Raman spectra are not due to a change in resonance condition but mainly due to the underlying isomerization reaction.

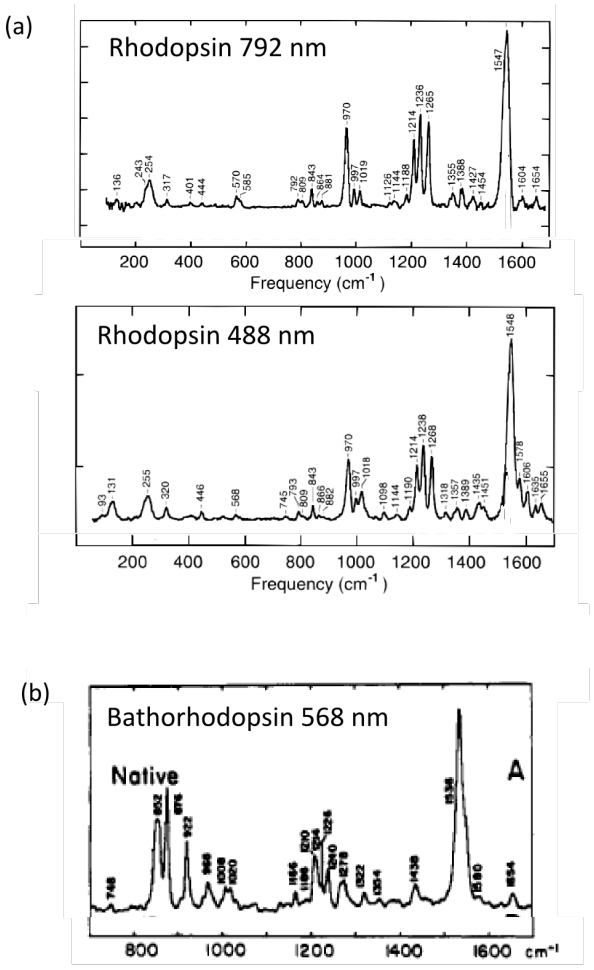

Figure S4: Overview of resonance Raman spectra at different excitation wavelength conditions. (a) Rhodopsin spectrum after pre-resonant (top, 792 nm) and resonant (bottom, 488 nm) excitation.[S7] (b) Bathorhodopsin spectrum after excitation at 568 nm.[S8] We note the very minor differences between spectra acquired at 792 and 488 nm compared to the very significant differences between rhodopsin and bathorhodopsin spectra.

Simulation of HOOP Motion

Previous studies using femtosecond stimulated Raman spectroscopy (FSRS) have shown, that in particular the HOOP region around 900 cm^{-1} undergoes significant frequency shifts, sensitive to the underlying isomerization reaction.[S3] The model put forward contains a set of three C-H wagging modes with an exponential change in frequency. To model the effect, such a frequency shift would have in our experiment, we adopted the revised model devised

by McCamant[S9] and simulated three C-H wagging modes with frequency shifts according to Fig. S5a. By combining the resulting oscillations, we are able to obtain a single coherence, as shown in Figure S5b (green). Application of an exponentially-modified Gaussian (EMG) window function (Figure S5b, orange) followed by Fourier transformation reveals the expected Fourier power spectrum (Figure S5c, orange). In addition to the model parameters given in Figure S5d,[S9] we additionally have to assume an initial phase for each oscillation at a time delay of 200 fs. Without loss of generality, we assumed a phase of zero for the C_{10}-H and C_{11}-H while a phase of π was chosen for C_{12}-H. The latter phase was chosen to be out of phase with the C_{11}-H vibration to ensure that the respective hydrogen atoms move away from each other to lead to an isomerization. If the hydrogen atoms were to start in phase, no net isomerization would occur on the reaction time scale of photoexcited rhodopsin. Comparison to the experimental data, analyzed in the same way shows excellent agreement in the 860 cm^{-1} band. However, the lack of the C_{11}-H mode at 920 cm^{-1} cannot be explained by this model, providing additional evidence for the effect of a CI on a vibrational wavepacket in a coupling mode. We note, that the observed line shape of the 860 cm^{-1} mode in the Fourier power spectrum was not reproducible if we assumed phases of zero, π and zero for the C_{10}-H, C_{11}-H and C_{12}-H modes instead.

To trace potential frequency shifts, we performed a sliding window Fourier transform (SWFT) on this model (Figure S6, left), a model with non-shifting, stationary oscillations at bathorhodopsin HOOP frequencies (Figure S6, middle), and our experimental data (Figure S6, right). The Fourier power spectrum as a function of the window position is obtained and scaled to the maximum for each window time, removing exponential decay dynamics for clarity. We observe only minor differences between between the two sets of simulated data, both showing clear signatures of the C_{11}-H mode at 920 cm^{-1}. In contrast, the experimental data never shows the appearance of this mode, strengthening the proposed coupling mode mechanism. Residual oscillations in the SWFT of the measured data are mainly caused by the interference with the residual rhodopsin mode at 970 cm^{-1}.

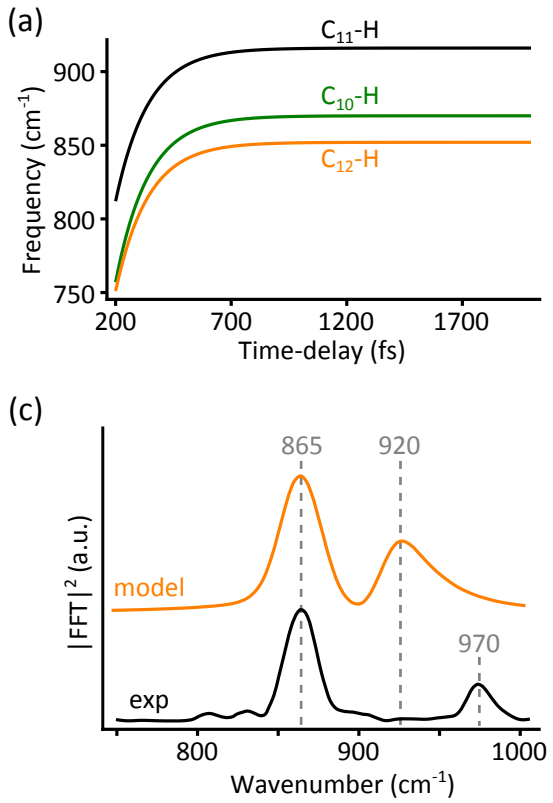

(d)

Parameter	Value
Time constant spectral upshift (fs)	140
vibrational dephasing time (fs)	620
Frequency C_{10}-HOOP initial (cm^{-1})	757
Frequency C_{10}-HOOP final (cm^{-1})	870
Frequency C_{11}-HOOP initial (cm^{-1})	812
Frequency C_{11}-HOOP final (cm^{-1})	916
Frequency C_{12}-HOOP initial (cm^{-1})	751
Frequency C_{12}-HOOP final (cm^{-1})	852
EMG time constant (fs)	500
EMG rise time (fs)	45

Figure S5: Simulation details of HOOP evolution. (a) Time-dependent frequency shifts for hydrogen wagging motions C_{10}-H, C_{11}-H and C_{12}-H. (b) Resulting overall coherent oscillation (green, top) and EMG windowed oscillation (bottom, gray and orange, respectively). (c) Obtained Fourier power spectra of simulated data (orange) compared to experimental results showing the lack of the 920 cm^{-1} C_{11}-H mode. (d) Overview over simulation parameters adapted from McCamant.[S9] Note that the relative initial phases have been assumed to be zero, zero and π for C_{10}-H, C_{11}-H and C_{12}-H modes to account for the overall isomerization process.

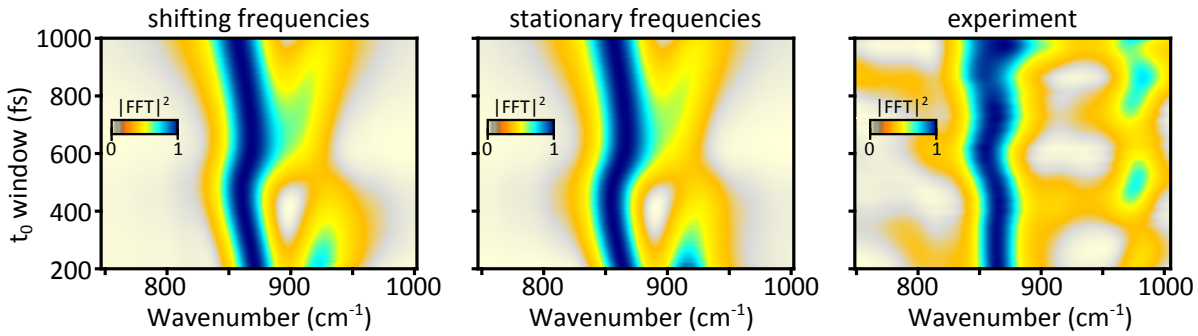

Figure S6: Sliding window Fourier transform analysis of the model presented in Figure S5 (left), a set of stationary bathorhodopsin modes (middle) and the experimentally observed data (right) as a function of the window time delay t_0. The spectra for each window time-delay have been normalized to the largest band for visibility purposes.

These results show, that the detection of frequency shifts in the time domain is very challenging. While in FSRS all oscillations are generated in phase when the Raman probe pulse interacts with the sample, we are initiating the coherence directly upon photoexcitation. Since we cannot temporally separate excitation and coherence generation, our method becomes less phase sensitive to the overall isomerization and provides spectral signatures dominated mainly by the bathorhodopsin photoproduct. However, it is this difference which allows us to obtain information on the CI by careful comparison to the reactant and product Raman spectra.

References

(S1) Liebel, M.; Kukura, P. *J. Phys. Chem. Lett.* **2013**, *4*, 1358–64.

(S2) Kovalenko, S. A.; Dobryakov, A. L.; Ruthmann, J.; Ernsting, N. P. *Phys. Rev. A* **1999**, *59*, 2369–84.

(S3) Kukura, P.; McCamant, D. W.; Yoon, S.; Wandschneider, D. B.; Mathies, R. A. *Science* **2005**, *310*, 1006–9.

(S4) Polli, D.; Lüer, L.; Cerullo, G. *Rev. Sci. Instrum.* **2007**, *78*, 103108.

(S5) Johnson, A. E.; Myers, A. B. *J. Chem. Phys.* **1996**, *104*, 2497–507.

(S6) Polli, D.; Brida, D.; Mukamel, S.; Lanzani, G.; Cerullo, G. *Phys. Rev. A* **2010**, *82*, 053809.

(S7) Lin, S. W.; Groesbeek, M.; van der Hoef, I.; Verdegem, P.; Lugtenburg, J.; Mathies, R. A. *J. Phys. Chem. B* **1998**, *102*, 2787–806.

(S8) Palings, I.; Pardoen, J. A.; Van den Berg, E.; Winkel, C.; Lugtenburg, J.; Mathies, R. A. *Biochemistry* **1987**, *26*, 2544–56.

(S9) McCamant, D. W. *J. Phys. Chem. B* **2011**, *115*, 9299–305.